Automatic network coupling analysis for dynamical systems based on detailed kinetic models

Dirk Lebiedz,* Julia Kammerer, and Ulrich Brandt-Pollmann
Interdisciplinary Center for Scientific Computing, Im Neuenheimer Feld 368, D-69120 Heidelberg, Germany
(Received 9 May 2005; published 12 October 2005)

We introduce a numerical complexity reduction method for the automatic identification and analysis of dynamic network decompositions in (bio)chemical kinetics based on error-controlled computation of a minimal model dimension represented by the number of (locally) active dynamical modes. Our algorithm exploits a generalized sensitivity analysis along state trajectories and subsequent singular value decomposition of sensitivity matrices for the identification of these dominant dynamical modes. It allows for a dynamic coupling analysis of (bio)chemical species in kinetic models that can be exploited for the piecewise computation of a minimal model on small time intervals and offers valuable functional insight into highly nonlinear reaction mechanisms and network dynamics. We present results for the identification of network decompositions in a simple oscillatory chemical reaction, time scale separation based model reduction in a Michaelis-Menten enzyme system and network decomposition of a detailed model for the oscillatory peroxidase-oxidase enzyme system.

DOI: 10.1103/PhysRevE.72.041911 PACS number(s): 82.39.−k, 82.40.−g, 82.39.Rt

I. INTRODUCTION

High-quality experimental data become increasingly available for detailed modeling of complex chemical reaction systems in both technical processes and cell biology. A central modeling task of general significance and interest is to identify the minimum kinetic model which can be used instead of the full reaction mechanism while retaining a desired degree of accuracy for the essential dynamical features. This is equivalent to identifying a network decomposition in terms of a submanifold on which the "dominant" part of the system dynamics takes place [1], which is a central problem in dynamical systems theory.

In systems biology [2], complexity and model reduction become increasingly important in particular for the analysis of large-scale biochemical networks. They require reliable and efficient numerical methods for both reducing the effective dimensionality of the models and identifying network modularizations and dynamical couplings between components as crucial guides on the way towards an elucidation of the systems' mechanistic functioning. A largely unsolved central problem is the final interpretation of numerical simulation results to obtain information about mechanistic aspects of a cellular process. The latter involves inter-alia the analysis of the kind and extent of interactions between network components and subsystems and other dynamical features that are finally related to physiological functions. However, these are largely obscured in high-dimensional phase space associated with detailed kinetic models and it is extremely difficult to extract useful information by simply looking at hundreds or thousands of time series for single biochemical species [3].

For these reasons, automatic numerical methods will be crucial to reduce the dimensionality of kinetic models as far as possible on the one hand and on the other hand to aid the identification of functional network decompositions by reducing the system's apparent complexity. Since in many biochemical and cellular processes multiple time-scales are involved, a reasonable approach is the identification of time-scale couplings for system analysis and potential elucidation of functional couplings of components or subsystems. As the time-scale composition of nonlinear ODE models may change significantly when trajectories propagate through phase space, a dynamical and local (pointwise) analysis performed online during numerical integration is necessary in most cases. In Ref. [4] a robust implementation of such a method and its application to a biochemical reaction network are described. Among the most common approaches to complexity reduction widely used for biochemical reaction networks are metabolic control analysis (MCA) [5,6] and stoichiometric network analysis (SNA) [7]. These techniques have recently been extended from the original application to steady-state conditions to transient dynamics [8,9]. The application of such methods to (bio)chemical reaction networks can provide considerable insight into the mechanism and associated significance of the network structure. For a review on applications see Ref. [10] and references therein. SNA can, for example, be exploited to analyze bifurcation behavior as a function of the network structure [11] or an identification of subnetworks [12]. Schreiber *et al.* address the important case of model construction/selection problems related to the probing of different proposed reaction mechanisms by help of SNA [13] for oscillatory enzyme systems, among them the peroxidase-oxidase (PO) reaction also treated in the present work (see Sec. III).

However, the insight provided by the previous methodologies into the quantitative dynamic phase space structure with respect to the relative time evolution of component interdependencies which would help significantly to identify dynamical coupling relations between network components is rather restricted. In order to make an attempt to complement the scope of successful static network topology and stoichiometry based methods, here, we present a generalized dynamic sensitivity analysis approach which is based on the dynamic coupling analysis of families of trajectories during the transient time evolution of a dynamical system. Our

*Electronic address: lebiedz@iwr.uni-heidelberg.de

analysis identifies a (local) minimal model dimension and the corresponding active dynamical modes that decouple from the remaining modes in the sense of a negligible effect of perturbations on the essential system dynamics.

II. METHOD AND ALGORITHM

Our numerical algorithm dynamically identifies mode decoupling during integration of trajectories in phase space based on the framework of a generalized sensitivity analysis. By relaxing and thus enslaving the dynamical modes with the smallest sensitivity coefficients with respect to the remaining ones, this decoupling is exploited for computing the minimal model dimension consistent with a user defined error tolerance. The final result of a subsequent singular value analysis is a network decomposition into modules. Mathematically the procedure corresponds to a piecewise approximation of a full ODE model by a differential algebraic equation (DAE) model with the algebraic part $0=g(y,z)$ representing the relaxation (enslavement) of modes with smallest sensitivities under the restriction of a desired accuracy for the remaining modes $y(t)$,

$$\dot{x}(t) = \frac{dx}{dt} = F(x)(\mathrm{ODE}) \rightarrow$$

$$\dot{y}(t) = \frac{dy}{dt} = f(y,z), 0 = g(y,z)(\mathrm{DAE}). \qquad (1)$$

From the geometric viewpoint the DAE can be interpreted as an ODE on a manifold described by the algebraic equations.

Compared to the local time-scale concept developed in Ref. [4], our approach is not restricted to local time-scale decoupling but can in principle identify any form of dynamical decoupling on any finite time horizon in terms of a sensitivity analysis along state trajectories.

The central task in our analysis is the identification of the large and small sensitivity modes and the decision which of the latter can be assumed to be relaxed (enslaved) without causing a too large error in the remaining modes. The algorithm we introduce here presents a robust strategy for solving this problem numerically and exploiting the results for the identification of component and subnetwork decoupling in the full kinetic model under consideration. Our complexity reduction method is based on the computation of sensitivities along pieces of a nominal trajectory (on time horizon $[0,T]$) providing information on the propagation behavior of small perturbations of the initial value with the phase flow (approximated by accurate numerical integration) in a first order (linear) approximation. The final property of interest is the derivative (sensitivity) of the endpoint of a small trajectory piece with respect to the initial value. This can be formulated as

$$\delta x(T) = W(T)\,\delta x(0),\ W(T) := \frac{\partial x(T)}{\partial x(0)}. \qquad (2)$$

$\delta x(0)$ and $\delta x(T)$ are the initial and final perturbations of the values $x(0), x(T)$, the latter being located on the nominal trajectory in the time interval $[0,T]$. This sensitivity matrix $W(T)$ can be computed by integrating $\dot{x}=F(x)$ numerically from slightly perturbed initial values $x(0)+\delta x(0)$ and evaluate finite difference schemes involving the difference between perturbed and nominal final values divided by the absolute value of the initial perturbation $\delta x(T)/\delta x(0)$ for all coordinate directions. Here, modern adaptive step-size integrators are required for efficient numerical simulation of stiff and large-scale chemical reaction models. Since the output of such numerical integration of a trajectory piece does usually not depend continuously on the input (initial value) due to error-adaptive switches in integrator step size and/or order, a naive use of finite differences may lead to severe numerical problems and low accuracy of the sensitivity information [14]. In order to compensate such inaccuracies it can be shown that an integrator accuracy close to the machine precision (eps) is required for sensitivity accuracies of the order $\sqrt{(eps)}$ [15]. Therefore, this external numerical differentiation generally results in unacceptable long integration times for large-scale stiff systems.

The internal numerical differentiation (IND) technique suggested by Bock [16] avoids these disadvantages by freezing the discretization scheme obtained by step-size adaptive and error-controlled integration of the nominal trajectory and using this fixed scheme also for the perturbed trajectories. In this case an integrator accuracy of $\sqrt{(eps)}$ is enough for obtaining derivatives in the same accuracy range [16]. IND has been implemented in the efficient and robust numerical integrator DAESOL [17] which is based on a BDF method (backward differentiation formula) particularly suitable for stiff ODE and DAE systems. We use DAESOL as part of our algorithm for computing nominal trajectories and sensitivities piecewise on predefined equidistant time intervals $[0,T],[T,2T], \ldots$. The length of these intervals represents the minimal time-scale resolution of our method meaning that (de)couplings below this step size cannot be resolved. The final sensitivity output for a trajectory piece is the matrix $W(T)$ in (2) which will be abbreviated as W in the following.

A well-known theorem in linear algebra [18] assures the existence of a singular value decomposition for each regular matrix $W \in \mathbb{R}^{n\times n}$, meaning the existence of orthogonal matrices U and V and a diagonal matrix Σ with

$$W = U \times \Sigma \times V^T, \quad \Sigma = \mathrm{diag}(\sigma_i), \quad i = 1,\ldots,n \qquad (3)$$

and the singular values $\sigma_i > 0$ in the matrix Σ. It follows directly from the orthogonality of the matrices U and V that the image of the unit sphere under the operation of W is a hyperellipse (Fig. 1) because V^T represents rotation of the original coordinate axes without affecting angles and lengths, the diagonal matrix Σ stretches or contracts the axes and U rotates again [18]. The column vectors u^j of U, the left singular vectors, correspond to the half-axes of the image hyperellipse. This means that they represent those directions in phase space in which a contraction/expansion of the initial perturbation occurs with a factor σ_i on time horizon $[0,T]$. Due to the orthogonality of U these axes are pairwise orthogonal vectors (Fig. 1). The singular values describe the relative contraction and/or expansion behavior (dynamics of

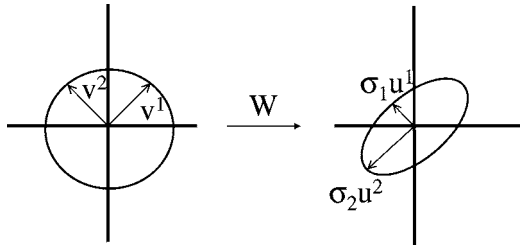

FIG. 1. Mapping of a unit sphere of initial perturbations to a hyperellipse by the propagator matrix W according to Eq. (2). In the singular value decomposition (3) of W the left singular vectors u^i correspond to the semiaxes of the ellipse whereas the right singular vectors v^i are the preimages of u^i under the linear map W and thus correspond to those perturbations in phase space contracting or expanding with the factor σ_i, $Wv^i=\sigma_i u^i$. The shortest semiaxes correspond to the fastest contracting directions (those modes with the smallest sensitivities with respect to the remaining ones).

the distance) of trajectories without taking twisting around each other into account.

In the next step the original ODE model is transformed by an orthogonal coordinate transformation with U^T which rotates the original axes into the direction of the left singular vectors. Then it is assumed that the dynamical modes in the strongest contracting phase space direction u^k (the shortest semiaxis of the hyperellipse image $Wv^k=\sigma_k u^k$ with smallest σ_k) are fully relaxed already at the initial value. This is equivalent to setting the scalar product projection of the ODE vector field onto this direction to zero,

$$g = u^k F(x) = 0. \tag{4}$$

The result is a DAE system of type (1) in transformed coordinates

$$(\dot{y},\dot{z}) = U^T\dot{x} = U^T F = (f,g) = (f,0) \tag{5}$$

with $(n-1)$ differential variables y and one algebraic variable z. The algebraic part can be interpreted as defining the essential dynamics manifold in phase space enslaving the corresponding dynamical modes to the remaining ones, $y=h(z)$. Here lies the connection to many previously described model reduction techniques based on time-scale separation or similar concepts like intrinsic low dimensional manifolds (ILDM) [19], computational singular perturbation (CSP) [20], minimal entropy production trajectories (MEPT) [21], Fraser's algorithm [22,23], sensitivity analysis approaches [24,25], and others (see Refs. [26–28] for a comprehensive overview). Among the first methods for model reduction in chemical kinetics were the classical quasisteady state and partial equilibrium approximations [29–33], lumping techniques [34,35] and sensitivity analysis [36,37]. Subsequently computational methods have been developed which include the ILDM [19,38,39], CSP methods [20,40,41], inertial manifold approaches [42], dynamic dimension reduction [4,43], ideas from optimization [44], statistical mechanics approaches to extract essential information from models and data [45], iterative trajectory based methods to find attracting manifolds [22,23,46–48] and thermodynamic projection operator methods [49], to name just the most important which came into broader applications. Many of these methods aim at computing slow attracting manifolds that bundle trajectories in phase space and describe the essential "long-term" dynamics of the system assuming fast dynamical modes to be relaxed. Since fast dynamical modes cause strong contraction in the corresponding phase space direction, this is a special case of our more general sensitivity based approach as will be demonstrated for a simple biochemical enzyme system later.

The main feature of the method presented here is a combination of flow-maps and their derivative with orthogonal coordinate transformation based singular value decomposition, error-controlled maximal relaxation of dynamical modes and finally computation of unique contributions of each chemical species to the mutually orthogonal active and relaxed subspace decomposition. The final results provide useful insight into the dynamic network coupling structure as demonstrated for three example applications in the next section.

For the computation of consistent initial conditions for the DAE system (1) which correspond to a point on the "slaving" manifold $0=g(y,z)$, we start from the original ODE initial value $(y(0),z(0))=U^T x(0)$ fixing the variables $y(0)$ and relaxing $z(0)$ to $z_{\mathrm{relax}}(0)$ by solving the nonlinear equation system (4). This is done by a generalized Newton iteration with a homotopylike continuation method implemented within the DAESOL code [17]. In order to check if the relaxation assumption for the direction of strongest contraction z and therefore the replacement of the full ODE model by a DAE approximation (1) is allowed we introduce a suitable error criterion. After integration of both the transformed ODE and DAE systems from the original initial value $(y(0),z(0))=U^T x(0)$ and the consistent initial value $(y(0),z_{\mathrm{relax}}(0))$, respectively, on the same time horizon $[0,T]$ we require for the relative error in the remaining differential variables (active modes)

$$\frac{|y_i^\star(T)-y_i(T)|}{|y_i(T)|} \leqslant y_{TOL}, \quad i=1,\ldots,n-1 \tag{6}$$

with $y_i^\star(T)$ denoting the solution of the DAE approximation and $y_i(T)$ the solution of the transformed full ODE. If the error is less or equal to a user defined desired accuracy y_{TOL}, the decoupling (reduction of differential variables by one) is accepted on the considered time horizon and the whole procedure is repeated with the second strongest contraction direction. The algorithm runs iteratively until the error criterion is no longer fulfilled and the resulting DAE system is considered to be the maximally reduced model with $rd=n-a$ (reduced dimension) differential variables and a algebraic ones on $[0,T]$. Then the procedure is repeated for the next interval $[T,2T]$ with the previous minimal dimension as a starting guess that is stepwise increased if necessary and decreased if possible to save computational effort.

The algorithm offers the possibility of dynamic error-controlled model reduction of ODE systems with the time horizon T determining the desired resolution. Even more important, it allows to analyze time-scale couplings of single species and/or subsystems of species by exploiting the infor-

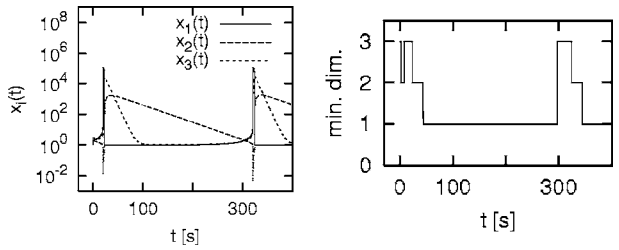

FIG. 2. Left-hand side, numerical simulation of the Oregonator model (8) using DAESOL [17]. Right-hand side, minimum dimension for the model (8) as a function of time for approximately 1.3 oscillation periods computed by the presented algorithm with an error tolerance $y_{TOL}=10^{-2}$ in (6) and minimum resolution $T=2.0$ [see (2)].

mation in the matrix U which contains those directions in which perturbations decay strongly without much affecting the dynamical behavior of the less contracting or the expanding directions. When taking these directions u^j as new coordinate axes for the transformed system they can be represented as linear combination of the "old" coordinate axes corresponding to the original chemical species. Thus a relative contribution r_i (in %) of each original coordinate i to the subspace of active dynamical modes (corresponding to new coordinate directions, $u^j, j=1,\ldots,rd$) can be determined by computing the projection of the species coordinate vector onto the active modes subspace, taking the norm of this projection and dividing by the sum of this norm and the norm of the projection into the relaxed subspace,

$$r_i := \frac{\left\| \sum_{j=1}^{rd} u_i^j u^j \right\|}{\left\| \sum_{j=1}^{rd} u_i^j u^j \right\| + \left\| \sum_{j=rd+1}^{n} u_i^j u^j \right\|}, \quad i = 1,\ldots,n. \tag{7}$$

with u_i^j denoting the ith component of the column vector u^j. Thus we identify a relative contribution of each species to the active dynamics manifold (see, e.g., Fig. 3).

III. RESULTS AND DISCUSSION

We demonstrate the performance of our method by analyzing a simple model system which displays oscillatory dynamical behavior,

$$\frac{dx_1}{dt} = 77.27[x_2 + x_1(1 - 8.375 \times 10^{-6} x_1 - x_2)],$$

$$\frac{dx_2}{dt} = \frac{1}{77.27}[x_3 - (1 + x_1)x_2],$$

$$\frac{dx_3}{dt} = 0.161(x_1 - x_3),$$

$$(x_1(0), x_2(0), x_3(0)) = (1,2,3). \tag{8}$$

This is a variant of the Oregonator model [50] for the oscillating Belousov-Zhabotinsky reaction. Figure 2 shows

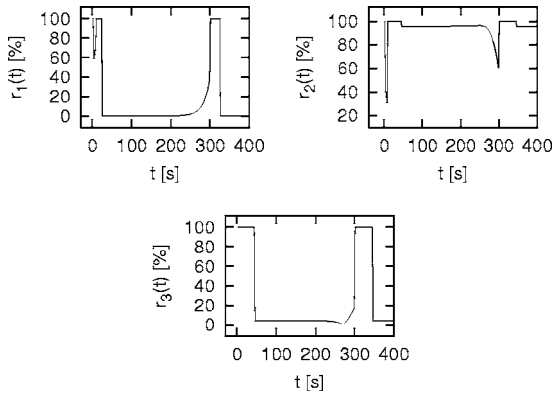

FIG. 3. Oregonator model, Relative contribution $r_i(t)$ of each chemical species x_i, $i=1$, 2, 3 in % to the subspace of active rd dynamical modes j with corresponding singular vectors u^j according to Eq. (7).

the minimal dimension of the reduced model computed by our algorithm along a periodic trajectory. Only during small parts of the closed phase space orbit are all three variables strongly coupled. In large parts a single active mode is sufficient to describe the complete dynamics accurately whereas all other modes can be treated as relaxed.

Figure 3 shows the result of the component analysis (7) demonstrating that the variables x_1 and x_3 are in a good approximation effectively decoupled because they share only a small contribution to the remaining single active mode. Due to the orthogonality of the singular vector axes a small contribution to the active modes means a large contribution to the fast contracting modes that can be regarded as relaxed (enslaved). This feature is of central importance for our approach since previous methods like ILDM or CSP that use similar mathematical techniques to project the system dynamics to a low dimensional manifold are restricted to nonorthogonal coordinate transformations. In the latter case a determination of contributions of single system components to the active and relaxed dynamical modes would not be uniquely possible. Thus, the final result of our algorithm is the identification of subsequent dynamic decoupling of two network components in the Oregonator system and this fits very well to the results of the numerical simulation for the full model (Fig. 2) where between $t=0$ and $t=100$ a subsequent relaxation of x_1 and x_3 can be observed. The results for this example application from chemical kinetics demonstrate the value of our model and complexity reduction approach for the identification of network couplings in complex dynamical systems. It may turn out to be valuable for the analysis of large biochemical networks and provide in particular important insight into the dynamical structure of their high-dimensional phase space and potential network modularizations. To underline the specific suitability of our method for biochemical reaction networks we present further results for a simple Michaelis-Menten enzyme system

$$E + S \overset{k_{\pm 1}}{\leftrightarrow} ES \overset{k_2}{\rightarrow} E + P \tag{9}$$

described by the ordinary differential equation system,

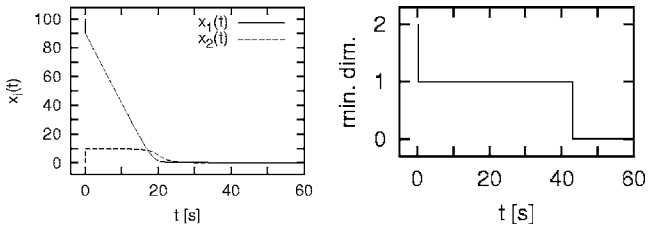

FIG. 4. Left-hand side, numerical simulation of the Michaelis-Menten model (10) using DAESOL [17]. Right-hand side, minimum dimension for the model (8) as a function of time for approximately 1.5 oscillation periods computed by the presented algorithm with an error tolerance $y_{TOL}=10^{-2}$ in (6) and minimum resolution $T=0.3$ [see (2)].

$$\frac{dx_1}{dt} = -k_1(E_T - x_2)x_1 + k_{-1}x_2,$$

$$\frac{dx_2}{dt} = k_1(E_T - x_2)x_1 - k_2x_2 - k_{-1}x_2, \tag{10}$$

with $x_1=[S], x_2=[ES]$ (substrate and enzyme-substrate-complex concentrations, respectively), $[E_T]=[E]+[ES]=100.0$ (total enzyme concentration), rate coefficients $k_1=1.0, k_{-1}=1.0, k_2=0.5$ and initial conditions $x_1(0)=100.0, x_2(0)=0$.

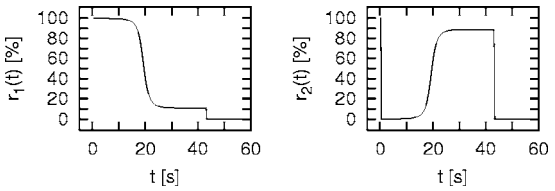

FIG. 5. Michaelis-Menten model, relative contribution $r_i(t)$ of each chemical species x_i, $i=1, 2$ in % to the subspace of active *rd* dynamical modes j with corresponding singular vectors u^j according to Eq. (7).

The computational results of our algorithms (Figs. 4 and 5) show that the method successfully identifies a time scale decoupling and confirms the widely used quasi-steady-state assumption for the enzyme-substrate complex. Furthermore the algorithm reliably identifies the validity range of the QSSA demonstrating that it is not appropriate in the transient initial phase and the final phase where most of the substrate has been consumed. In between, the contribution of the enzyme-substrate-complex dynamics to the slow (active) subspace is very small and the full dynamics are governed by the substrate. The plateau between 0 and 20 s represents the

TABLE I. Detailed model of the peroxidase-oxidase reaction coupled to the activation of an enzyme *Enz*. The initial condition values are 12.0 μM for O_2 and 1.5 μM for Per^{3+}, all other initial concentrations are zero.

Reaction [a]	Rate expression	Constant
(1) $NADH+O_2+H^+ \rightarrow NAD^+ + H_2O_2$	$k_1[NADH][O_2]$	3.0 [b]
(2) $H_2O_2+Per^{3+} \rightarrow coI$	$k_2[H_2O_2][Per^{3+}]$	1.8×10^7 [b]
(3) $coI+NADH \rightarrow coII+NAD^{\cdot}$	$k_3[coI][NADH]$	4.0×10^5 [b]
(4) $coII+NADH \rightarrow Per^{3+}+NAD^{\cdot}$	$k_4[coII][NADH]$	2.6×10^5 [b]
(5) $NAD^{\cdot}+O_2 \rightarrow NAD^+ + O_2^-$	$k_5[NAD^{\cdot}][O_2]$	2.0×10^7 [b]
(6) $O_2^-+Per^{3+} \rightarrow coIII$	$k_6[O_2^-][Per^{3+}]$	1.7×10^6 [b]
(7) $2O_2^-+2H^+ \rightarrow H_2O_2+O_2$	$k_7[O_2^-]^2$	2.0×10^7 [b]
(8) $coIII+NAD^{\cdot} \rightarrow coI+NAD^+$	$k_8[coIII][NAD^{\cdot}]$	11.0×10^7 [b]
(9) $2NAD^{\cdot} \rightarrow NAD_2$	$k_9[NAD^{\cdot}]^2$	5.6×10^7 [b]
(10) $Per^{3+}+NAD^{\cdot} \rightarrow Per^{2+}+NAD^+$	$k_{10}[Per^{3+}][NAD^{\cdot}]$	1.8×10^6 [b]
(11) $Per^{2+}+O_2 \rightarrow coIII$	$k_{11}[Per^{2+}][O_2]$	1.0×10^5 [b]
(12) $\rightarrow NADH$	k_{12}	0.132
(13) $O_2(gas) \rightarrow O_2(liquid)$	$k_{13}[O_2]_{eq}$	4.4×10^{-3} [de]
(−13) $O_2(liquid) \rightarrow O_2(gas)$	$k_{-13}[O_2]$	4.4×10^{-3} [d]
(14) $Enz_{inact}+O_2^- \rightarrow Enz_{act}$	$\frac{k_{14}[O_2^-]^5}{(K_f^5+[O_2^-]^5)}$	0.005 [b] (k_{14})
		0.4 [cf] (K_f)
(15) $Enz_{act} \rightarrow Enz_{inact}$	$k_{15}[Enz_{act}]$	1.6 [d]

[a] Per^{3+} and Per^{2+} indicate iron(III) and iron(II) peroxidase, respectively. coI, coII, and coIII indicate the enzyme intermediates compound I, compound II, and compound III.
[b] In $M^{-1}\ s^{-1}$.
[c] In M.
[d] In s^{-1}.
[e] The value of $[O_2]_{eq}$ is 12 μM.
[f] The amount of Enz_{inact} is assumed to be large compared to Enz_{act} and therefore considered to be constant, total concentration included in rate constant k_{14}.

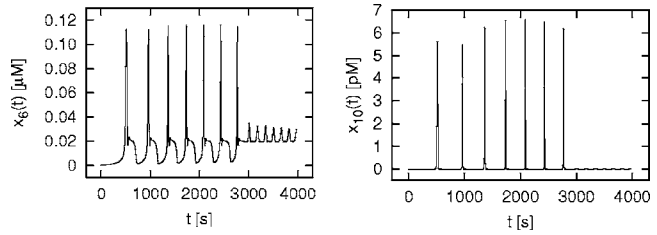

FIG. 6. Numerical simulation of the PO model (Table I) using DAESOL [17]. Left-hand side, species $x_6(t)$, superoxide ion O_2^-; Right-hand side, species $x_{10}(t)$, coupled enzyme Enz_{act}.

regime where the QSSA for the enzyme-substrate complex is valid due to the high turnover of its formation and dissociation. Later, the restricted substrate availability is the rate limiting factor and the essential system dynamics is dominated by the rate of decay of the enzyme-substrate complex. The results for the Michaelis-Menten system are not surprising at all, but nicely demonstrate that our algorithm is able to identify all aspects of the well-known coupling behavior that is widely exploited in modeling single-enzyme systems.

In order to demonstrate successful applicability to more complex (bio)chemical reaction mechanisms we analyze a detailed model (Table I) of the PO enzyme system [51], see [52] for a comprehensive overview related to the PO system. For our decomposition analysis, we artificially add a hypothetical enzyme component *Enz* to the core model that is activated by superoxide ions. These ions are known to play a role as signaling molecules in immune responses which are closely related to the PO reaction [53]. The latter serves for the production of reactive oxygen intermediates (ROI) in a respiratory burst response of immune cells aimed at pathogen destruction in intracellular phagosomes. Figure 6 shows the rich dynamical behavior observed for this enzyme system ranging from relaxation oscillations to harmonic oscillations and steady state behavior (long term regime, not shown). We assume highly cooperative activity of the added superoxide activated enzyme *Enz* with a Hill coefficient $n=5$ (see reaction 14 in Table I). Figure 8 depicts the results of the component analysis showing the contribution of the chemical species NAD H_2O_2 and the activated enzyme Enz_{act} to the active subspace for the computed minimum model dimension (Fig. 7). Obviously these components decouple from the rest of the network and for all of them a nearly identical contribution pattern is observed (see Fig. 8). For comparison

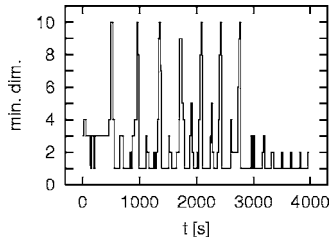

FIG. 7. Minimum dimension for the PO model (Table I) as a function of time for two different dynamical regimes (relaxation oscillations, $0 \leqslant t \leqslant 2800$ s, and harmonic oscillations, $t \geqslant 2800$ s, see also Fig. 6), $y_{TOL}=10^{-2}$ in (6) and minimum resolution $T=20.0$ [see (2)].

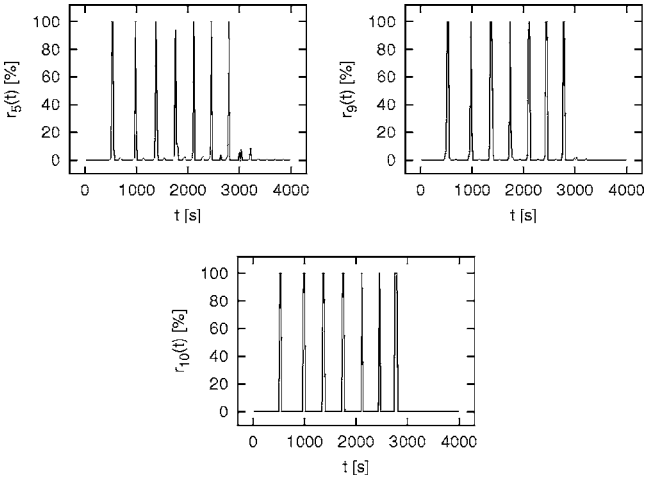

FIG. 8. PO model, relative contribution $r_i(t)$ of the chemical species x_i, $i=5$, NAD; $i=9$, H_2O_2; $i=10$, Enz_{act} in % to the subspace of active *rd* dynamical modes j with corresponding singular vectors u^j according to Eq. (7).

Fig. 9 shows the corresponding active mode contribution of NADH. The decoupling is expected for the enzyme component which has therefore been *a posteriori* coupled as an internal standard to the core PO system "by hand" to confirm that our analysis can successfully identify a subsystem (here a single enzyme) that is loosely coupled to the full reaction network. However, the components NAD and H_2O_2 seem to decouple as well meaning that a local change in their concentrations has very little effect on the dynamical behavior of the whole system. A decoupling of H_2O_2 has been described recently also as a result of a quasi-integral approach to chemical reaction network reduction [54]. NAD radicals, however, are known to be centrally involved in mediating an autocatalysis cycle within the PO reaction (see, for example, Ref. [13]). Nevertheless, their dynamics seem to decouple from the network in the sense that small perturbation locally do not affect the system dynamics essentially. This has been confirmed by numerical simulations introducing small perturbations of NAD concentrations at various time points. Except for small time horizons near the maximum amplitude of relaxation oscillations, the perturbed trajectories relax almost immediately to the unperturbed trajectory indicating a buffering mechanism for the effect of NAD radicals obviously caused by the interaction of the whole reaction network. Probably the decoupling is governed by the fast dynamics

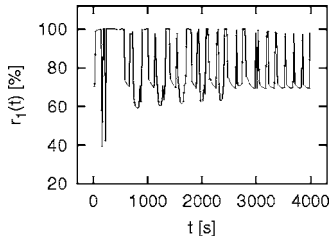

FIG. 9. PO model, for comparison with Fig. 8, relative contribution $r_1(t)$ of chemical species x_1, NADH in % to the subspace of active *rd* dynamical modes j with corresponding singular vectors u^j according to Eq. (7).

associated with the high reactivity of these radicals.

The minimum dimension analysis (Fig. 7) suggests that in large parts of the simulated time horizon less than four to five variables are sufficient to describe the overall dynamics accurately. Remarkably the full model is only required in dynamical regimes where the coupled enzyme is activated (Enz_{act}). However, this is not causally linked with the presence of the enzyme, the network analysis yields essentially the same results if the enzyme is removed from the PO model. The dimension of the full model is then nine and both reduced dimension and network coupling structure (data not shown) remain the same as in the previous case.

In large-scale complex biochemical networks the identification of dynamical coupling is by far not as obvious as in the Michaelis-Menten example system and the analysis of the PO system shows that in general possible decoupling cannot be identified intuitively by simply looking at the time series of species concentrations. The results promise wide ranging applicability to detailed realistic reaction mechanisms. In sum, our numerical algorithm may help significantly to identify and justify approximations aiming at model reduction on the one hand and to analyze the dynamical phase space structure on the other hand which provides important information on mechanistic aspects of dynamical functions and possible network modularization. Such kind of analysis is supposed to be a valuable tool for systems biology approaches.

ACKNOWLEDGMENT

The authors gratefully acknowledge Jürgen Warnatz, IWR Heidelberg, for financial and scientific support and Ursula Kummer and Jürgen Zobeley at EML Heidelberg for collaboration.

[1] J. Guckenheimer and P. Holmes, *Nonlinear Oscillations, Dynamical Systems and Bifurcation of Vectors Fields* (Springer, New York, 1997).
[2] H. Kitano, Nature (London) **420**, 206 (2002).
[3] M. R. Roussel and S. J. Fraser, Chaos **11**, 196 (2001).
[4] J. Zobeley *et al.*, Trans. Comput. Syst. Biol. **1**, 90 (2005).
[5] R. Heinrich and S. Schuster, *The Regulation of Cellular Systems* (Chapman and Hall, New York, 1996).
[6] D. A. Fell, Biochem. J. **286**, 313 (1992).
[7] B. L. Clarke, Cell Biophys. **12**, 237 (1988).
[8] B. P. Ingalls and H. M. Sauro, J. Theor. Biol. **222**, 23 (2003).
[9] J. J. Hornberg *et al.*, FEBS J. **272**, 244 (2005).
[10] J. Ross and M. O. Vlad, Annu. Rev. Phys. Chem. **50**, 51 (1999).
[11] P. Strasser, J. D. Stemwedel, and J. Ross, J. Phys. Chem. **97**, 2851 (1993).
[12] M. Eiswirth, A. Freund, and J. Ross, Adv. Chem. Phys. **80**, 127 (1991).
[13] I. Schreiber, Y.-F. Fen, and J. Ross, J. Phys. Chem. **100**, 8556 (1996).
[14] C. W. Gear and T. Vu, in *Numerical Treatment of Inverse Problems in Differential and Integral Equations*, edited by P. Deuflhard and E. Hairer (Birkäuser, Boston, 1983).
[15] J. Stoer and R. Bulirsch, *Introduction to Numerical Analysis* (Springer, New York, 1992).
[16] H. G. Bock, in *Modelling of Chemical Reaction Systems*, edited by K. H. Ebert, P. Deuflhard, and W. Jäger, Springer Series in Chemical Physics (Springer, Heidelberg, 1981).
[17] I. Bauer *et al.*, Astron. Astrophys. **317**, 273 (1997).
[18] L. N. Trefethen and D. Bau, *Numerical Linear Algebra* (SIAM, Philadelpia, 1997).
[19] U. Maas and S. B. Pope, Combust. Flame **88**, 239 (1992).
[20] S. H. Lam and D. A. Goussis, Int. J. Chem. Kinet. **26**, 461 (1994).
[21] D. Lebiedz, J. Chem. Phys. **120**, 6890 (2004).
[22] S. J. Fraser, J. Chem. Phys. **88**, 4732 (1988).
[23] M. R. Roussel and S. J. Fraser, J. Chem. Phys. **93**, 1072 (1990).
[24] A. S. Tomlin *et al.*, Combust. Flame **91**, 107 (1992).
[25] L. E. Whitehouse, A. S. Tomlin, and M. J. Pilling, Atmos. Chem. Phys. **4**, 3721 (2004).
[26] M. S. Okino and M. L. Mavrovouniotis, Chem. Rev. (Washington, D.C.) **98**, 391 (1998).
[27] A. N. Gorban, I. V. Karlin, and A. Y. Zinovyev, Phys. Rep. **396**, 197 (2004).
[28] A. S. Tomlin, T. Turányi, and M. J. Pilling, in *Low Temperature Combustion and Autoignition*, Comprehensive Chemical Kinetics Vol. 35, (Elsevier, Amsterdam, 1997) pp. 293–437.
[29] D. E. Koshland, Jr., J. Phys. Chem. **60**, 1375 (1956).
[30] R. H. Snow, J. Phys. Chem. **70**, 2780 (1966).
[31] T. Turányi, A. S. Tomlin, and M. J. Pilling, J. Phys. Chem. **97**, 163 (1993).
[32] K.-C. Chou, J. Biol. Chem. **264**, 12074 (1989).
[33] D. J. M. Park, J. Theor. Biol. **46**, 31 (1974).
[34] G. Li, H. Rabitz, and H. Toth, Chem. Eng. Sci. **46**, 95 (1991).
[35] G. Li, H. Rabitz, and H. Toth, Chem. Eng. Sci. **49**, 343 (1994).
[36] H. Rabitz, M. Kramer, and D. Dacol, Annu. Rev. Phys. Chem. **34**, 419 (1983).
[37] T. Turányi, J. Math. Chem. **5**, 203 (1990).
[38] U. Maas, Appl. Math. (Germany) **3**, 249 (1995).
[39] U. Maas, Comput. Visual. Sci. **1**, 69 (1998).
[40] M. Hadjinicolaou and D. A. Goussis, SIAM J. Sci. Comput. (USA) **20**, 781 (1999).
[41] A. Zagaris, H. G. Kaper, and T. J. Kaper, J. Nonlinear Sci. **14**, 5991 (2004).
[42] A. N. Yannacopoulos *et al.*, Physica D **83**, 421 (1995).
[43] P. Deuflhard and J. Heroth, *Scientific Computing in Chemical Engineering* (Springer, Heidelberg, 1998), p. 29.
[44] L. Petzold and W. Zhu, AIChE J. **45**, 869 (1999).
[45] K. S. Brown and J. P. Sethna, Phys. Rev. E **68**, 021904 (2003).
[46] A. H. Nguyen and S. J. Fraser, J. Chem. Phys. **91**, 186 (1989).
[47] M. R. Roussel and S. J. Fraser, J. Phys. Chem. **95**, 8762 (1991).
[48] R. T. Skodje and M. J. Davis, J. Phys. Chem. A **105**, 10356 (2001).
[49] A. N. Gorban, I. V. Karlin, V. B. Zmievskii, and S. V. Dymova,

Physica A **275**, 361 (2000).
[50] J. Field and R. M. Noyes, J. Chem. Phys. **60**, 1877 (1974).
[51] M. J. B. Hauser, U. Kummer, A. Z. Larsen, and L. F. Olsen, Faraday Discuss. **120**, 215 (2001).
[52] A. Scheeline *et al.*, Chem. Rev. (Washington, D.C.) **97**, 739 (1997).
[53] C. A. Janeway, P. Travers, and M. Walport, *Immunobiology* (Garland, London, 2004).
[54] R. Straube, D. Flockerzi, S. C. Müller, and M. J. B. Hauser, J. Phys. Chem. A **109**, 441 (2005).